Geophys. J. Int. (2004) **157,** 961–974 doi: 10.1111/j.1365-246X.2004.02273.x

Geoelectric dimensionality in complex geological areas: application to the Spanish Betic Chain

Anna Martí, Pilar Queralt and Eduard Roca

Departament de Geodinàmica i Geofísica, Universitat de Barcelona, C/Martí i Franquès s/n, 08028 *Barcelona, Spain. E-mail: anna@geo.ub.es*

Accepted 2003 December 11. Received 2003 December 11; in original form 2003 March 14

SUMMARY

Rotational invariants of the magnetotelluric impedance tensor may be used to obtain information on the geometry of underlying geological structures. The set of invariants proposed by Weaver *et al.* (2000) allows the determination of a suitable dimensionality for the modelling of observed data. The application of the invariants to real data must take into account the errors in the data and also the fact that geoelectric structures in the Earth will not exactly fit 1-D, 2-D or simple 3-D models.

In this work we propose a method to estimate the dimensionality of geoelectric structures based on the rotational invariants, bearing in mind the experimental error of real data. A data set from the Betic Chain (Spain) is considered.

We compare the errors of the invariants estimated by different approaches: classical error propagation, generation of random Gaussian noise and bootstrap resampling, and we investigate the matter of the threshold value to be used in the determination of dimensionality. We conclude that the errors of the invariants can be properly estimated by classical error propagation, but the generation of random values is better to ensure stability in the errors of strike direction and distortion parameters. The use of a threshold value between 0.1 and 0.15 is recommended for real data of medium to high quality. The results for the Betic Chain show that the general behaviour is 3-D with a disposition of 2-D structures, which may be correlated with the nature of the crust of the region.

Key words: Betic Chain, geoelectric structure, magnetotelluric tensor, rotational invariants.

1 INTRODUCTION

Magnetotelluric (MT) data comprise impedance tensor values corresponding to the observation sites, for the periods measured. Prior to the interpretation of such data it is important to obtain information about the dimensionality of the geoelectric structure to be modelled and about the existence of phenomena such as galvanic distortion, which may need correction. Analysis of dimensionality is a powerful tool that may yield information such as the variation of strike direction with depth that can be correlated with different processes and structure in the Earth's crust and mantle (e.g. Marquis *et al.* 1995). Depending on the result of dimensionality analysis, MT data may be interpreted as being either 1-D, 2-D or 3-D. The importance of this is demonstrated by a 2-D interpretation of 3-D data being acceptable in some cases while not in others (Wannamaker 1999; Park & Mackie 2000; Ledo *et al.* 2002; Ledo 2004).

A number of strategies have been used to justify two-dimensionality, and then determine strike direction. Groom & Bailey (1989) presented a tensor decomposition for a 3-D/2-D superimposed model that allowed the retrieval of a strike value for the 2-D regional structure.

Another tool used to obtain information about dimensionality is based on the analysis of the rotational invariants, i.e. onsets of parameters computed from observed impedance tensor values that do not depend on the direction of the observing axes. A number of authors have proposed various invariants (Swift 1967; Berdichevsky & Dmitriev 1976; Bahr 1988; Lilley 1993, 1998a,b) that are useful for particular categories of dimensionality. Fischer & Masero (1994) argue the existence of eight invariants, seven independent and one dependent. Szarka & Menvielle (1997) determined a full set of MT tensor invariants and suggested their use for compact 3-D interpretation.

An advance was made by Weaver *et al.* (2000), which provided a method whereby dimensionality associated with an impedance tensor is characterized in terms of the annulment of some of the seven independent invariants (the WAL invariants hereafter). However, the dimensionality models as described are ideal and may not be well matched by real data, which are affected by errors that propagate to invariant values. Consequently, dimensionality may be poorly determined, and it is necessary to use a non-zero threshold value to classify the invariant values.

© 2004 RAS

Szarka & Menvielle (1997) and Weaver *et al.* (2000) have imaged 3-D synthetic models with invariant values, but have not fully taken into account a consideration of experimental data.

In this work, we consider the magnetotelluric data obtained from the central part of the Betic Chain. Using a subset of these data, a geoelectric 2-D model was constructed (Carbonell *et al.* 1998; Pous *et al.* 1999). However, since the regional structure of this area is very complex, it is possible that a 3-D interpretation of the full data set should be made. As a first step, an analysis of dimensionality is required. Accordingly, the aim of this work is twofold: (1) to use the WAL invariants to determine the geoelectric structure associated with data from the South of Spain, and to infer the possible geological implications and (2) to study the problems that arise with the calculation of rotational invariants with real data, and the manner in which these problems can be addressed. Specifically, these problems are the threshold values for the invariants and the error treatment of the data.

2 THE GEOELECTRIC DIMENSIONALITY

2.1 Theoretical background

In the magnetotelluric method, the time variation of the electric and magnetic fields recorded is converted to the frequency domain. Following WAL notation (Weaver *et al.* 2000), the horizontal complex components of the electric field $\vec{E}$ can be expressed in terms of those of the magnetic field $\vec{B}$ using the magnetotelluric (MT) tensor, $M(\omega)$, whose components M_{ij} are complex:

$$\begin{pmatrix} E_x(\omega) \\ E_y(\omega) \end{pmatrix} = \begin{pmatrix} M_{xx} & M_{xy} \\ M_{yx} & M_{yy} \end{pmatrix} \begin{pmatrix} B_x(\omega) \\ B_y(\omega) \end{pmatrix} \tag{1}$$

where x and y are the directions along which the electric and magnetic fields are measured. The expression of the MT tensor in another reference frame, $x'\, y'$, is $M' = R_\theta \cdot M \cdot R^T{}_\theta$, where R_θ is a matrix for clockwise rotation through angle θ:

$$R_\theta = \begin{pmatrix} \cos\theta & \sin\theta \\ -\sin\theta & \cos\theta \end{pmatrix}. \tag{2}$$

The components of the MT tensor are expressed in units of electrical resistance, ohm (Ω), and their values are determined by the electrical properties of the subsurface.

The MT tensor presents characteristic features regarding the dimensionality, which can be 1-D, 2-D or 3-D (Vozoff 1986, 1991), depending on the type of geoelectric structure over which the measurements have been carried out.

The observed data are often affected by galvanic telluric distortion, a phenomenon produced by the presence of local bodies near the surface (Jones 1983; Jiracek 1990). As a consequence of galvanic distortion, the measured impedance tensor may display a 3-D form, although information on 1-D or 2-D regional structure can be retrieved (Bahr 1988). One of the most commonly used methods to remove the effects of distortion and to recover the regional tensor is the decomposition method of Groom & Bailey (1991), which can be employed when the regional structure is 2-D.

2.2 WAL invariants

Parameters which are invariant under the rotation of the impedance tensor (Vozoff 1972; Berdichevsky & Dmitriev 1976) allow the characterization of some tensor properties, especially those concerning aspects of dimensionality (Swift 1967; Bahr 1988). For example, seven independent rotational invariants of the impedance tensor ($Z = \mu_0 \cdot M$, where μ_0 is the magnetic permeability of free space) were defined by Szarka & Menvielle (1997): det(Re(Z)), det(Im(Z)), Im(det(Z)), Re($Z_{xy} - Z_{yx}$), Im($Z_{xy} - Z_{yx}$), Re($Z_{xx} + Z_{yy}$) and Im($Z_{xx} + Z_{yy}$).

Some rotational invariants are null for particular dimensionality models, and a number of authors have proposed combinations of invariants (Bahr 1988, 1991; Szarka 1999) to indicate whether a measured tensor corresponds to a given type of structure. Weaver *et al.* (2000) also employed a set of seven rotational invariants (termed here as the WAL invariants and denoted I_1 to I_7). The expressions of the WAL invariants are as follows, where the MT tensor components are decomposed and separated into real and imaginary parts:

$$M = \begin{pmatrix} \zeta_1+\zeta_3 & \zeta_2+\zeta_4 \\ \zeta_2-\zeta_4 & \zeta_1-\zeta_3 \end{pmatrix} = \begin{pmatrix} \xi_1+\xi_3 & \xi_2+\xi_4 \\ \xi_2-\xi_4 & \xi_1-\xi_3 \end{pmatrix} + \begin{pmatrix} \eta_1+\eta_3 & \eta_2+\eta_4 \\ \eta_2-\eta_4 & \eta_1-\eta_3 \end{pmatrix} i \tag{3}$$

$$I_1 = \left(\xi_1^2 + \xi_4^2\right)^{1/2}, \quad I_2 = \left(\eta_1^2 + \eta_4^2\right)^{1/2} (\mathrm{m\,s^{-1}}) \tag{4}$$

$$I_3 = \frac{\left(\xi_2^2 + \xi_3^2\right)^{1/2}}{I_1}, \quad I_4 = \frac{\left(\eta_2^2 + \eta_3^2\right)^{1/2}}{I_2} \tag{5}$$

$$I_5 = \frac{\xi_4\eta_1 + \xi_1\eta_4}{I_1 I_2}, \quad I_6 = \frac{\xi_4\eta_1 - \xi_1\eta_4}{I_1 I_2} = d_{41} \tag{6}$$

$$I_7 = (d_{41} - d_{23})/Q \tag{7}$$

Table 1. Dimensionality criteria according to the invariant values of the magnetotelluric tensor.

Case	Invariants	Dimensionality	
1	$I_k = 0\ (k = 3-7)$	1-D	
2	$I_3 \neq 0$ or $I_4 \neq 0$	2-D (if $d_{23} = 0$)	
3	$I_3 \neq 0$ or $I_4 \neq 0$ and $I_5 \neq 0$	(a) 3-D/2-D (only twist) (if $I_7 = 0$)	
		(b) 3-D/2-D or 3-D/1-D (if I_7 undefined)	
4	$I_3 \neq 0$ or $I_4 \neq 0$, $I_5 \neq 0$ and $I_6 \neq 0$	3-D/2-D	
5	$I_7 \neq 0$ (with or without galvanic distortion)	3-D	

where

$$d_{ij} = \frac{\xi_i \eta_j - \xi_j \eta_i}{I_1 I_2} \text{ and } Q = \left[(d_{12} - d_{34})^2 + (d_{13} + d_{24})^2\right]^{1/2} \tag{8}$$

are also invariants that depend on the other ones. If Q is too small, then I_7 approaches infinity and its value remains undetermined. (Note that I_3 to I_6 are normalized, and that I_3 to I_7 and Q are dimensionless).

Invariants I_1 and I_2 provide information about the 1-D magnitude and phase of the geoelectrical resistivity:

$$\rho = \mu_0 \frac{\left(I_1^2 + I_2^2\right)}{\omega}, \quad \varphi = \arctan\left(\frac{I_2}{I_1}\right) \tag{9}$$

while I_3 to I_7 are related also to the dimensionality of the geoelectric structures detected, and make it possible to establish criteria (Weaver *et al.* 2000, and Weaver personal communication 2003) that are suitable for assessing dimensionality and galvanic distortion (Table 1).

In cases with 2-D dimensionality the strike direction (θ), can be computed from the real or imaginary parts of the MT tensor components (θ_1 and θ_2),

$$\tan 2\theta_1 = -\frac{\xi_3}{\xi_2}, \quad \tan 2\theta_2 = -\frac{\eta_3}{\eta_2} \tag{10}$$

and in cases with galvanic distortion, the strike (θ) and distortion parameters (ϕ_1 and ϕ_2) (Smith 1995) can be retrieved (cases 3 and 4 in Table 1):

$$\tan 2\theta_3 = \frac{d_{12} - d_{34}}{d_{13} + d_{24}} \tag{11}$$

$$tan\, \phi_1 = \frac{\mathrm{Re} M'_{yy}}{\mathrm{Re} M'_{xy}} = \frac{\mathrm{Im} M'_{yy}}{\mathrm{Im} M'_{xy}} \tag{12}$$

$$\tan \phi_2 = \frac{\mathrm{Re} M'_{xx}}{\mathrm{Re} M'_{yx}} = \frac{\mathrm{Im} M'_{xx}}{\mathrm{Im} M'_{yx}}. \tag{13}$$

ϕ_1 and ϕ_2 are related to twist (θ_t) and shear (θ_e) angles (Groom and Bailey, 1989) through the expressions

$$\theta_t = \frac{\Phi_1 + \Phi_2}{2} \quad \text{and} \quad \theta_e = \frac{\Phi_1 - \Phi_2}{2}. \tag{14}$$

3 DIMENSIONALITY CRITERIA USING REAL DATA

The main problem when WAL invariant criteria are used with real noisy data is that the geoelectric dimensionality may be found to be 3-D, although other evidence suggests that a 1-D or 2-D interpretation would be valid for modelling. This is because invariant values for real data are in general never precisely zero. Weaver *et al.* (2000) address this problem by introducing a threshold value beneath which the invariants are taken to be zero. The threshold value they suggest is 0.1, which, although subjective, has been tested using a synthetic model with 2 per cent noise. Since the data addressed below have a higher percentage of error which propagates to the invariants, we need to redefine this threshold value, taking into consideration the invariants values and their errors.

Using WAL criteria with the threshold defined, if the dimensionality obtained is 2-D or 3-D/2-D (cases 2, 3a and 4 in Table 1), the strike directions and distortion parameters must be estimated with their errors. To address these matters we performed different tests to estimate the invariants and related parameters and their errors, and to chose an optimum threshold value. These tests were carried out using some of the MT data from the Betic Chain, with sites denoted as b01, b23 and b40. The corresponding geological setting and data acquisition is explained in Section 4.

3.1 Estimation of the invariants and their errors

The estimation of the values and errors of the invariants and related parameters depends on the values of the MT tensor components, computed from the spectra, and their errors. These errors are expressed as variances, computed using the method of Gamble *et al.* (1979), after assuming that noise is independent of the signals and stationary, and consequently that the components of M are statistically independent. To estimate all the invariants and related parameters and errors, three different approaches were tested: classical error propagation, random Gaussian noise generation and resampling methods:

(a) Classical error propagation. In this case, the values of the invariants are the named true values (hereafter I), computed directly from the expressions (3)–8). For small errors, the uncertainty of any function $y = f(x_1, x_2, \ldots, x_n)$ can be obtained from a Taylor expansion in terms of the errors ($\delta x_1, \delta x_2, \ldots, \delta x_n$) in the estimated variables $x_1, x_2, \ldots, x_n$. Using a first-order expansion, the error (δI) of each invariant (I) and the errors of the strike and distortion parameters are expressed as functions of the partial derivatives of the corresponding function and the variances of the components of M. The errors of the invariants were obtained as a function of ξ_i and η_i to simplify the expressions, and are summarized in the Appendix.

(b) Random Gaussian noise generation. This statistical approach is an alternative to the first one, which can fail when the errors in M are large. The problem lies in the lack of knowledge about the statistical distribution of M, since the only available data are the mean and variances of their components. Some authors assume a Gaussian distribution of M to compute new parameters and study their stability (Jones & Groom 1993; Weaver *et al.* 2000), or to obtain their probability functions and confidence limits (Lezaeta 2002), both from synthetic and real data. Thus, one way to estimate the invariants and their errors is to generate a set of n possible values of the M components, assuming Gaussian noise, around their true values, with the variances of the MT tensor components. This is done in order to obtain a set of possible values of the invariants. After obtaining this set of n realizations of each invariant for a determined site and period, its mean value (I') and standard deviation ($\sigma_{I'}$) are computed. The number n must be large enough to avoid biases between the true value (I) and mean value (I') of the invariant. The criterion to fix the optimum number n is to ensure that the difference between $I$and I' is no greater than the standard deviation:

$$\left|I - I'\right| \leq \sigma_{I'}. \tag{15}$$

The same procedure can be used to obtain the mean value and standard deviation of the strike direction and the distortion parameters.

(c) Resampling methods. The bootstrap method in particular (Efron & Tibshirani, 1998) uses a hypothetical population constructed from the recorded data and does not assume any statistical distribution. Thus, different statistical parameters can be computed from a larger number of samples. In our case the hypothetical sample consists of n' populations with m different samples each taken randomly from the population generated in approach (b). Subsequently, the total population is formed by $n' \times m$ samples. The invariants and their errors are obtained similarly to approach (b), as the mean values and standard deviations.

We present one example that compares the estimation of the invariants and their errors using these three approaches, corresponding to all the recorded periods of site b23 used in the Betic Chain magnetotelluric study. The variances in the magnetotelluric tensor correspond approximately to 1 per cent noise for the shortest periods, and increase up to 30 per cent for the longest ones.

The invariant values and error bars (Fig. 1)employing the three approaches are very similar and the errors resemble those of the components of the magnetotelluric tensor, which increase with the period. This behaviour, also observed at other sites of the data set, is a typical consequence of the loss of information when recording long-period bands. However, invariants I_7 and Q show the largest bias and disparity between the error bars of the three approaches. These errors are considerable since they correspond to the most unstable parameters (Weaver *et al.* 2000).

As a result, since the three approaches give similar error bars, we decided to employ approach (a) to estimate the invariants and their errors in order to avoid the possible biases that appear with approaches (b) and (c). The strike directions and distortion parameters, which depend on the derivatives of inverse trigonometric functions, have large error bars when these are computed using classical error propagation, especially when the errors of the tensor components are considerable. These values are better constrained with the generation of random values (approach b).

3.2 The threshold value

For the determination of the dimensionality using WAL invariants, it is necessary to decide if an invariant can be considered null or not. This is a compromise between the threshold value (τ hereafter) and the error bar of each invariant. We adopted the following criteria:

(1) To ascertain whether I_7 is undefined or not, by observing the values of Q and I_7:

(1.a) $Q < 0.1$ and/or $I_7 > 1 \Rightarrow I_7$ is undefined.
(1.b) $Q > 0.1$ and $I_7 < \tau \Rightarrow I_7 \approx 0$.
(1.c) $Q > 0.1$ and $I_7 > \tau \Rightarrow I_7 \neq 0$.

(2) For the rest of the invariants, I_3 to I_6, we establish whether these are null or not by considering the possible values of I_i and σ_i (Fig. 2):

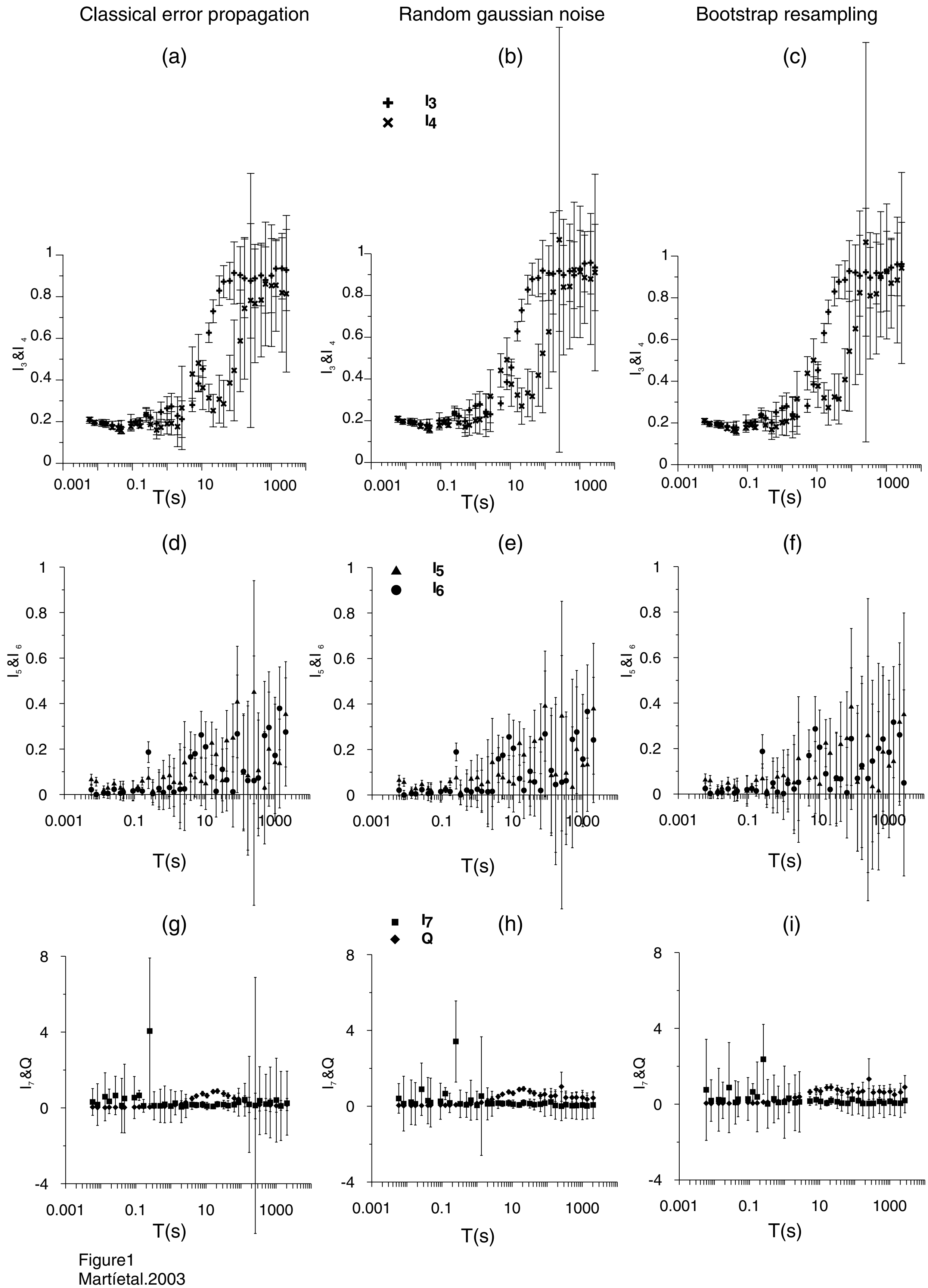

Figure 1. Invariant values at site b23 and their errors computed in three ways: classical error propagation, random Gaussian noise (1000 realizations) and bootstrap resampling (50 realizations for each of 200 samples): I_3 and I_4 (a), (b) and (c); I_5 and I_6 (d), (e) and (f); I_7 and Q (g), (h) and (i).

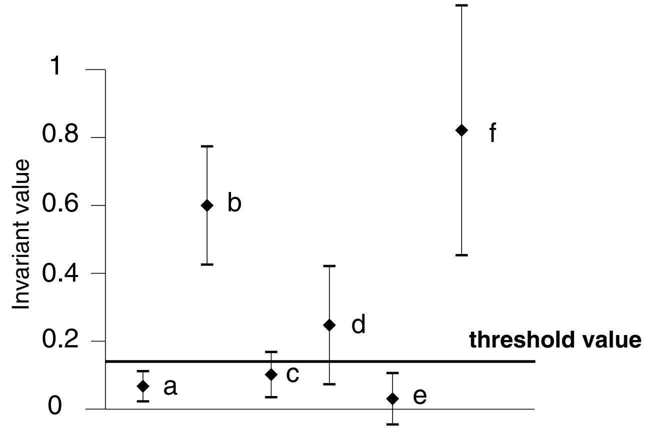

Figure 2. Different possibilities for the invariant values and their errors (τ = threshold value): (a) $I_i - \sigma_i < \tau$ and $I_i + \sigma_i < \tau$; (b) $I_i - \sigma_i > \tau$ and $I_i + \sigma_i > \tau$; (c) $I_i < \tau$ and $I_i + \sigma_i > \tau$; (d) $I_i > \tau$ and $I_i - \sigma_i < \tau$; (e) $I_i - \sigma_i < 0$; (f) $I_i + \sigma > 1$. Only in case (a) is the particular invariant considered to be zero.

(2.a) $I_i - \sigma_i$ and $I_i + \sigma_i < \tau \Rightarrow I_i \approx 0$ (Fig. 2a).
(2.b) $I_i > \tau$ and $I_i - \sigma_i > \tau \Rightarrow I_i \neq 0$ (Fig. 2b).
(2.c) $I_i < \tau$ and $I_i + \sigma_i > \tau \Rightarrow I_i \neq 0$ (Fig. 2c) (note that I_i would be regarded null if we had not taken the error into account).
(2.d) $I_i > \tau$ and $I_i - \sigma_i < \tau \Rightarrow I_i \neq 0$ (Fig. 2d).
(2.e) $I_i - \sigma_i < 0 \Rightarrow I_i$ is undefined (Fig. 2e).
(2.f) $I_i + \sigma_i > 1 \Rightarrow I_i$ is undefined (Fig. 2f).

If any of the invariants I_3 to I_6 is undefined (2.e and 2.f) the dimensionality of the corresponding tensor cannot be determined.

The choice of the threshold value τ is a subjective decision, but it is easy to test an appropriate range of values that works. A high value of τ gives the result that the invariants are considered null, resulting in too simple a structure (1-D for all sites and periods). On the contrary, a small value of τ implies that the invariants cannot be considered null and it gives rise to a more complex structure (3-D in general).

The WAL dimensionality analysis for different threshold values for a subset of the Betic data was done in order to find the optimum value that gives a dimensionality pattern which is stable and consistent, taking into account the errors of the invariants. The threshold values tested were 0.08, 0.1, 0.12, 0.15, 0.2 and 0.3.

Fig. 3 shows the dimensionality cases obtained for three representative sites and for each threshold value. The cases that were undetermined due to the errors are also included, the number of which decreases as the threshold value increases. However, with independence on the threshold value, dimensionality remains undetermined for those periods with relative errors in the MT tensor components greater than approximately 30 per cent.

The extreme values, $\tau = 0.08$, 0.2 and 0.3, provide dimensionality patterns which are inconsistent. However, intermediate values, $\tau = 0.1$, 0.12 and 0.15, give a quite stable pattern and a characteristic behaviour can be observed at any site. Site b01 reflects a 3-D/2-D dimensionality for some periods up to 0.12 s using $\tau = 0.1$, 0.12 and 0.15. Site b23 appears as 2-D up to 0.2 s, for any threshold value, and as 3-D/2-D for longer periods up 50 s, using $\tau = 0.12$, 0.15 and even 0.2. Site b40 shows a 1-D dimensionality at short periods (up to 1 s) for the three intermediate τ values. Consequently, for the studied sites, threshold values between 0.1 and 0.15 are the ones that give a better description of the dimensionality.

In the following, for all the periods of these three sites, we performed two kinds of analysis: in analysis A, we determined the strike directions and errors corresponding to a 2-D structure (θ_1 and θ_2 in eq. 10); in analysis B, we assumed a 3-D/2-D structure, computing the strike and distortion angles and their errors (θ_3 in eq. 11 and θ_t and θ_e in eq. 14). The strikes and errors obtained with both analyses allowed us to constrain the frequencies for which a strike direction and/or distortion parameters can be determined. If θ_1 and θ_2 are similar, with constant values and small error bars, the structure can be considered 2-D. If it is θ_3 that has small error bars and constant values of distortion angles, it can be considered 3-D/2-D. For the analysed sites the main results are:

(1) Site b01 (Fig. 4) : Analysis A (Fig. 4a) gives a good determination of the strike directions up to 200 s, where the errors in θ_1, and θ_2 become large. However, since values θ_1, θ_2 are dissimilar, it cannot correspond to a 2-D structure. Analysis B (Fig. 4b) shows large error bars, except for the period ranging between 0.02 s and 0.2 s, which can be described as 3-D/2-D because θ_3 and the distortion angles have a constant value.

(2) Site b23: Analysis A gives a good determination of the strike for the lowest periods up to 0.2 s, which have the same value $\theta_1 = \theta_2$ (Fig. 5a). Analysis B shows that constant strike direction and twist and shear angles can be inferred between 5 s and 50 s (Fig. 5b).

(3) Site b40: neither analysis A or B nor the computation of θ_1, θ_2 and θ_3 (Figs 6a and b) give a good determination of a possible 2-D or 3-D/2-D structure. However, up to periods of about 1 s, the MT tensor corresponds to a 1-D case ($M_{xy} = -M_{yx}$ and $M_{xx} = M_{yy} = 0$), and the computed apparent resistivities (Fig. 6c) and phases (Fig. 6d) have the same value for *xy* and *yx* modes. These values are the same as those obtained from invariants I_1 and I_2 (eq. 9). This is consistent with a 1-D interpretation of the data for the short and middle periods of this site.

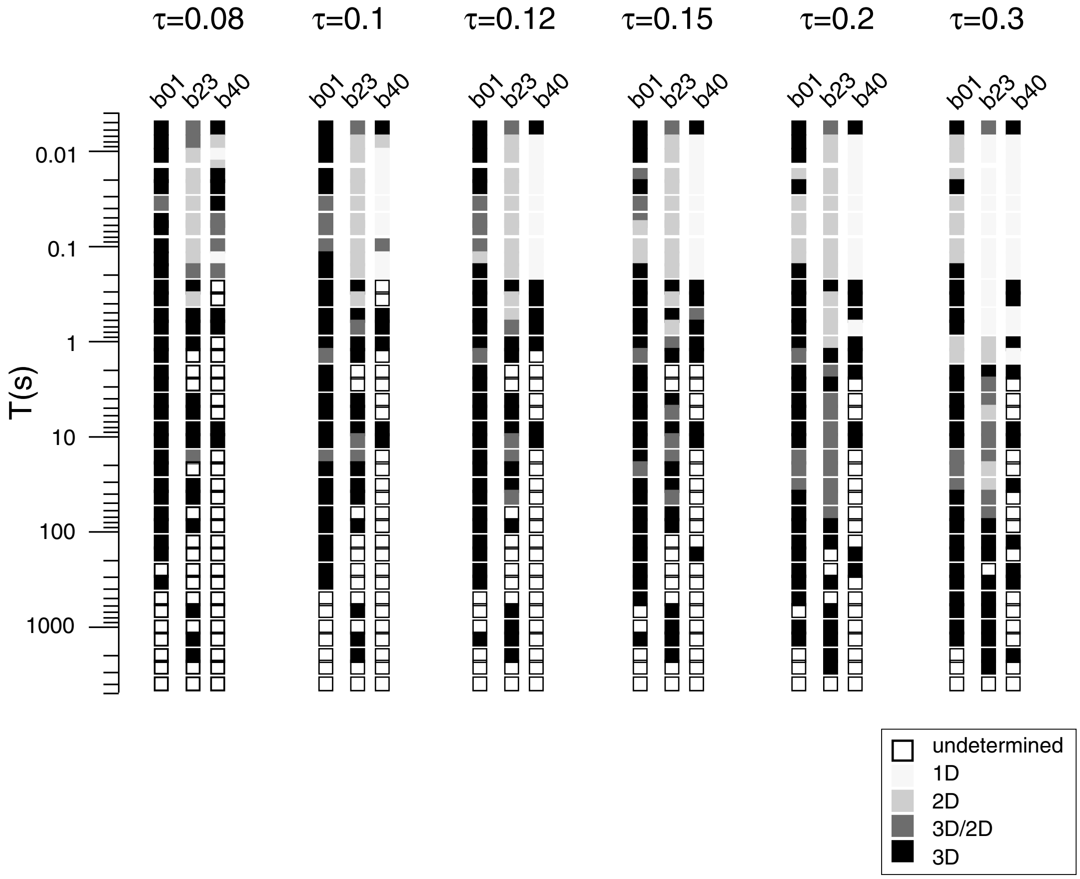

Figure 3. Dimensionality cases for sites b01, b23 and b40 from the Betics MT data set using different threshold values: 0.08, 0.1, 0.12, 0.15, 0.20 and 0.30.

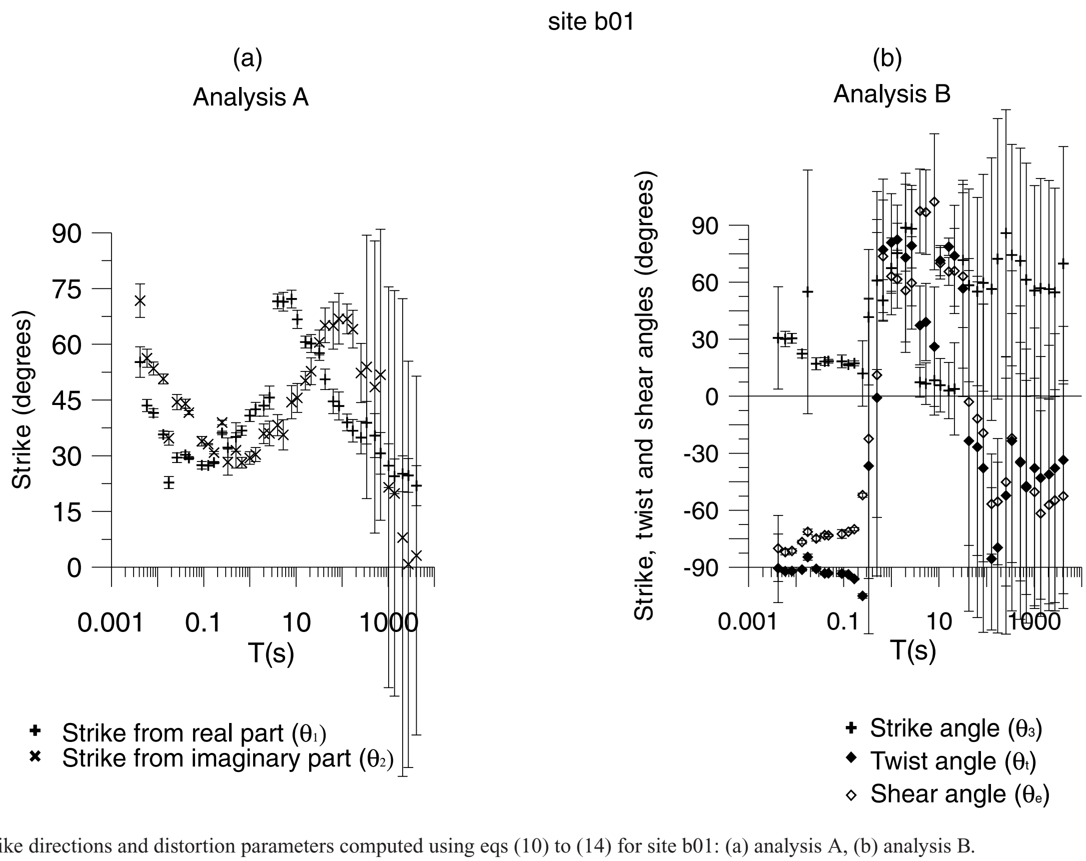

Figure 4. Strike directions and distortion parameters computed using eqs (10) to (14) for site b01: (a) analysis A, (b) analysis B.

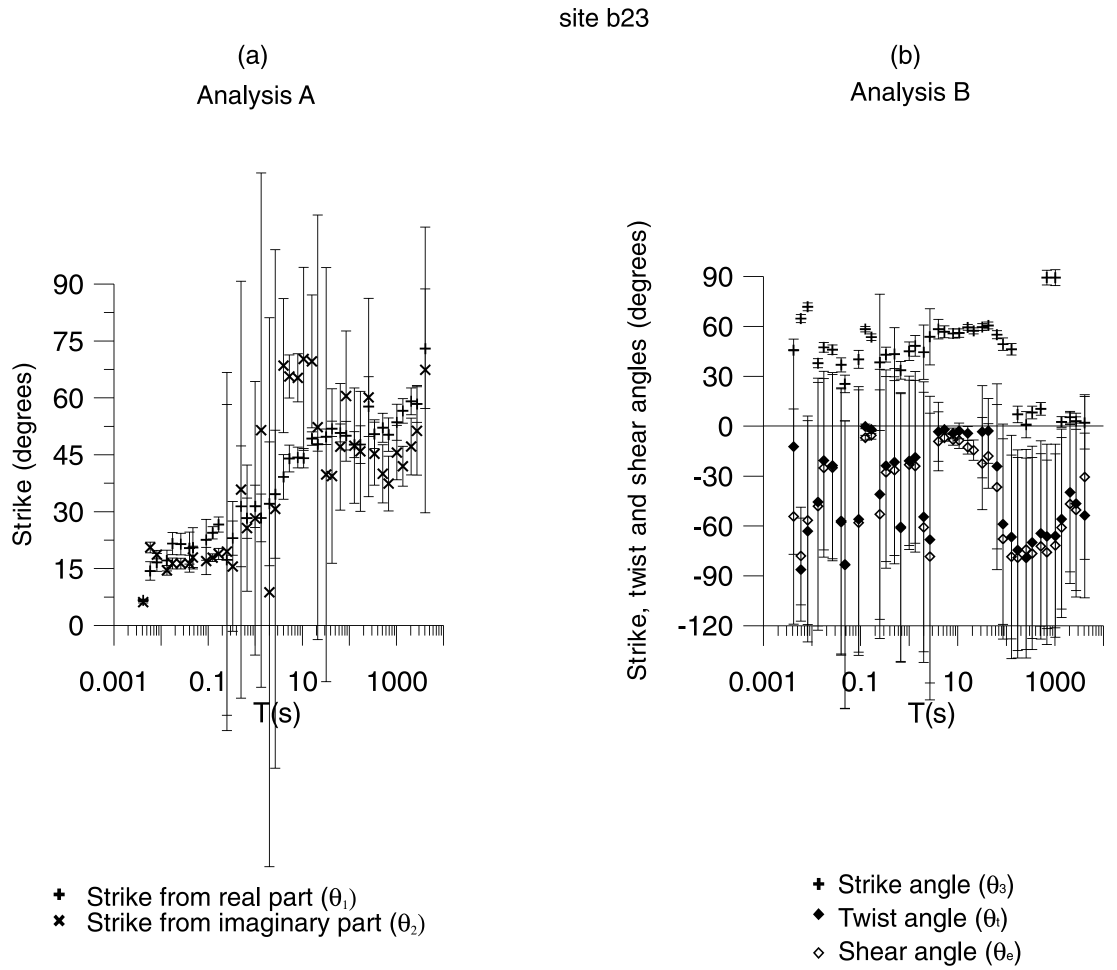

Figure 5. Strike directions and distortion parameters computed using eqs (10) to (14) for site b23: (a) analysis A, (b) analysis B.

The results from these analyses correspond to the dimensionality obtained using thresholds values between 0.1 and 0.15. Thus, we conclude that this threshold range is appropriate for a dimensionality analysis for data with up to 30 per cent noise in the impedance tensor components.

In order to corroborate these results, the Groom and Bailey decomposition for these three site was done using the Multisite multifrequency tensor decomposition code of McNeice & Jones (2001). The results are consistent with the previous ones, and for the specific range of periods where the behaviours are 2-D or 2-D/3-D the strikes coincided within the error bars.

3.3 Practical criteria

After performing these tests on the error treatment and the threshold value, we give these final recommendations:

(1) Determine the errors of the invariants using any of the described approaches (a), (b) or (c) in Section 3.1. However approach (a) is recommended to avoid biases.

(2) Determine the dimensionality using WAL criteria with a threshold value between 0.1 and 0.15, letting I_7 be undetermined if Q is below 0.1, and giving consideration to the error bars. Note that dimensionality will be well determined when relative errors in M are no greater than approximately 30 per cent.

(3) Compute the strike directions and/or distortion angles corresponding to 2-D and 3-D/2-D cases and their errors, using random noise generation.

4 APPLICATION TO REAL DATA: THE BETIC CHAIN

4.1 Geological setting

The Betic Chain (Fig. 7) is located in the south of the Iberian Peninsula, and represents the westernmost part of the Alpine Orogen Belt. Together with the African Rift, it conforms an arc-shaped belt surrounding the present Alboran Basin, which was formed as a consequence

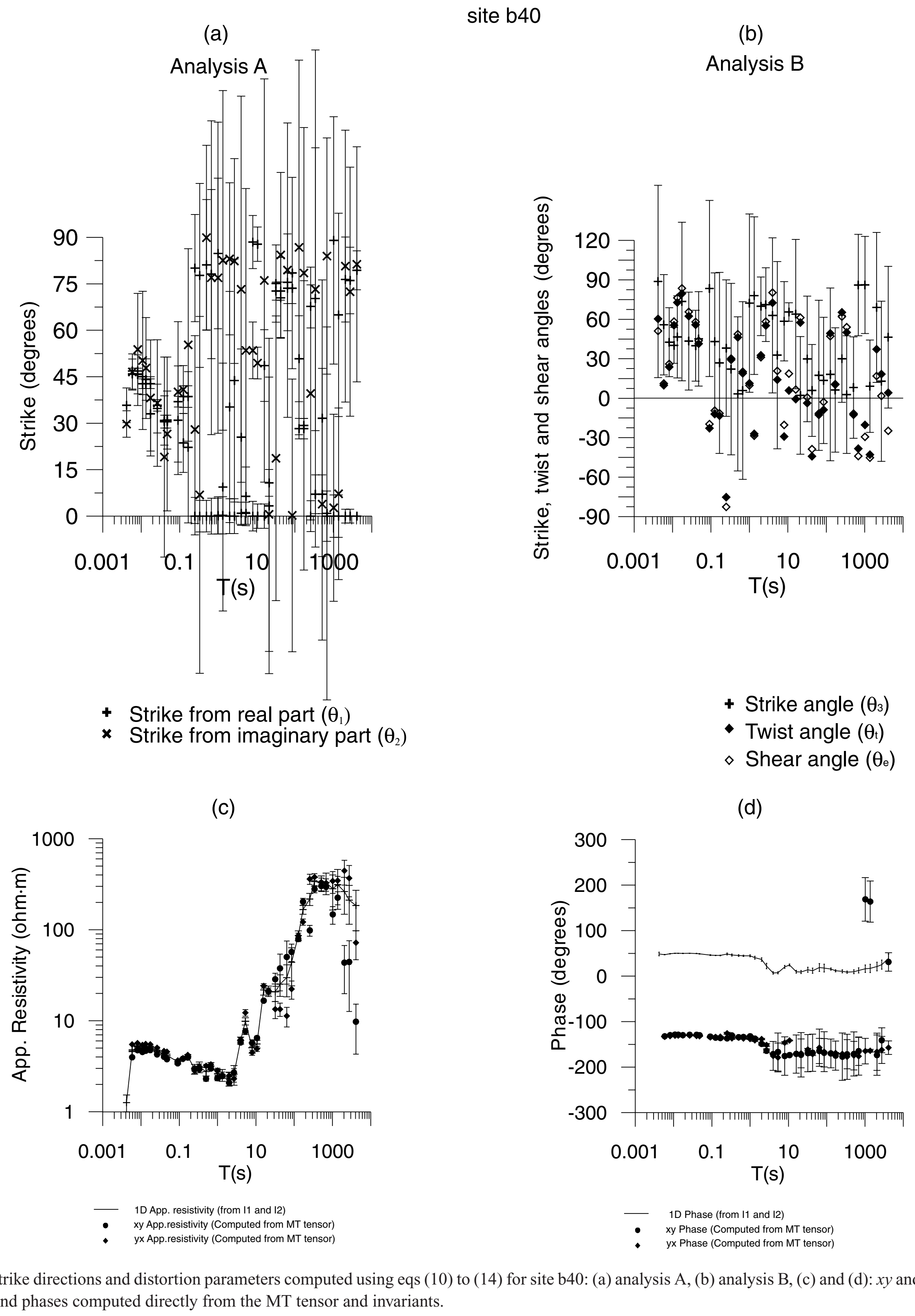

Figure 6. Strike directions and distortion parameters computed using eqs (10) to (14) for site b40: (a) analysis A, (b) analysis B, (c) and (d): *xy* and *yx* apparent resistivities and phases computed directly from the MT tensor and invariants.

of the convergence between the African and Iberian plates since the Late Cretaceous (Platt & Vissers, 1989; García-Dueñas *et al.*, 1992). The Betic Chain has been divided into external and internal zones. The external zone, located in the north and northeast, comprises a fold-and-thrust belt made up of Tertiary sediments and the allochthonous Mesozoic sedimentary cover of the South Iberian continental margin (García-Hernández *et al.* 1980), which overthrusted the Miocene Guadalquivir Foreland Basin. The internal zone, in the south, is more complex and is formed by three stacked metamorphic complexes that overthrusted the external zone during their emplacement in the

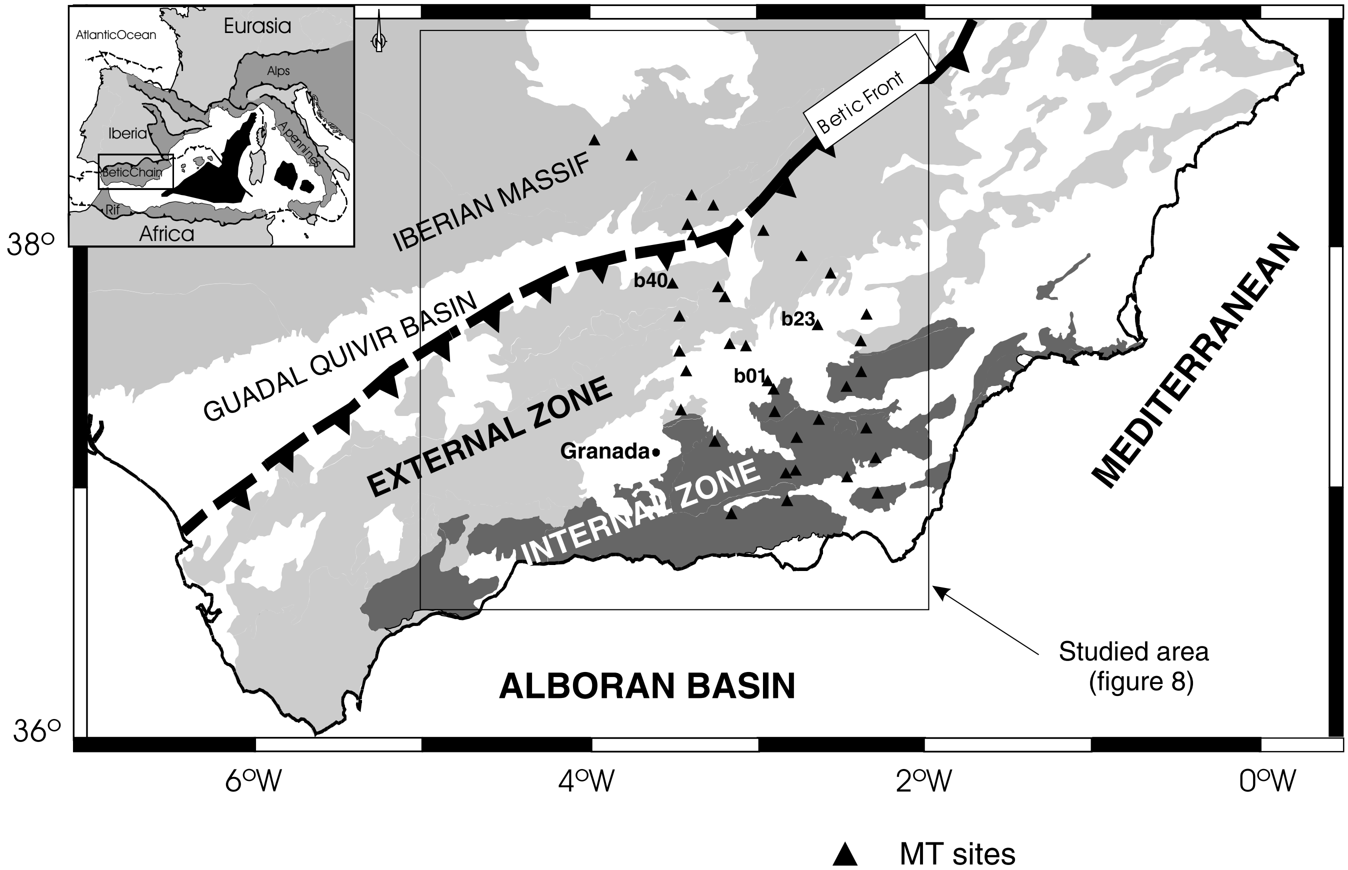

Figure 7. Geological setting and map of the Betics. The triangular symbols indicate the location of the magnetotelluric sites.

Late Cretaceous–Palaeogene periods. During the Early and Middle Miocene (Garcia-Dueñas *et al.* 1992; Johnson *et al.* 1997) this zone was affected by extension which led to the development of several intramontane basins filled with continental and marine Neogene and Quaternary sediments (Sanz de Galdeano & Vera 1992).

4.2 Magnetotelluric data

A magnetotelluric data survey was carried out in the central part of the Betic Chain between the Iberian Massif and the Alboran Sea. The analysed data correspond to 32 magnetotelluric sites located in the internal and external zones of the Betic Chain, the Guadalquivir Basin and the adjacent Iberian Massif. About 30 periods were recorded, from 0.004 to 4000 s, at each site. The data have good coherences and error bars in the impedance tensor components from 1 per cent to 30 per cent error.

The dimensionality analysis was carried out for every site and period. The true values of the invariant values were estimated and their errors were computed using classical error propagation. For the determination of the dimensionality we used a threshold value $\tau = 0.15$. Due to the errors, the dimensionality could not be determined for 30 per cent of the tensors, most of them associated with the longest periods.

5 RESULTS

For the cases in which the dimensionality could be determined it was synthesized in five categories: one dimensional (1-D), two-dimensional (2-D), two dimensional affected by galvanic distortion (3-D/2-D), three-dimensional (3-D), and the special case of galvanic distortion without a defined strike angle (3-D/2-D1-D).

In each site, these dimensionality categories were grouped in decade period bands (Fig. 8), in order to represent the prevalent categories and strikes at different penetrations. The average strike directions with their standard deviations were computed for the bands with 2-D or 3-D/2-D dimensionality. To solve the ambiguity in the determination of the strike direction, we took into account the induction arrows when available.

From the obtained results we can observe (Fig. 8) that the predominant dimensionality is 3-D, with abundant 1-D, 2-D and 3-D/2-D1-D structures for periods shorter than 1 s and rarer 3-D/2-D structures for periods between 1 and 1000 s.

Up to 1 s (bands 1, 2 and 3, Figs 8a to c), the dimensionality is significantly different between the Iberian Massif, the Betic Chain and the overlying Cenozoic basins. In the Iberian Massif, the structures are 3-D and above all 2-D with strike orientations going from ENE–WSW to

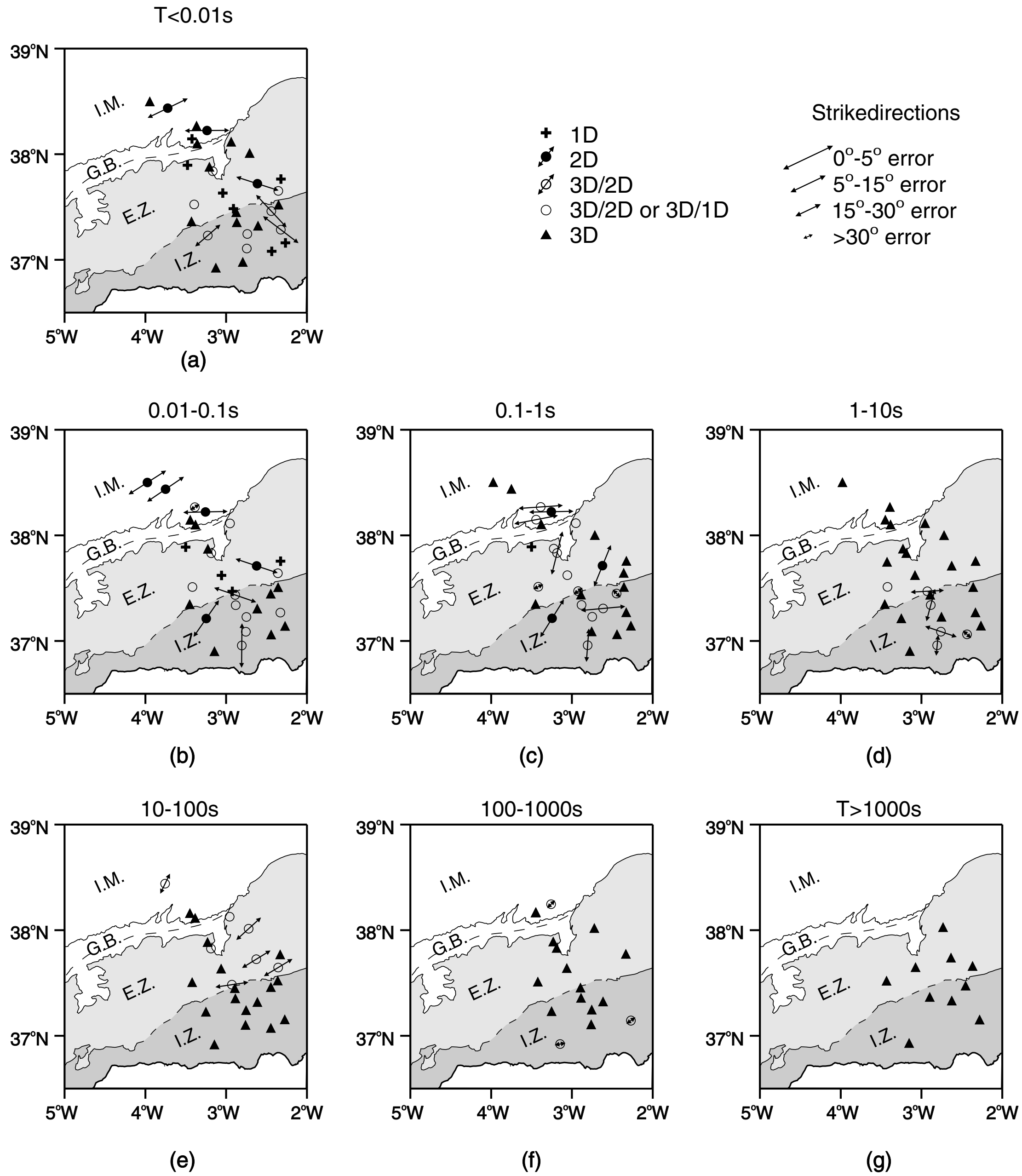

Figure 8. Dimensionality results grouped in seven period bands. Those cases in which the dimensionality could not be determined are not shown. The arrows indicating the strike directions are scaled by the inverse of the error in the determination of the strike: (a) band 1: $T < 0.01$ s; (b) band 2: 0.01 s – 0.1 s; (c) band 3: 0.1 s –1 s; (d) band 4: 1 s – 10 s; (e) band 5: 10 s – 100 s; (f) band 6: 100 s – 1000 s; (g) band 7: $T > 1000$ s. I.M.: Iberian Massif, G.B.: Guadalquivir Basin, E.Z.: External Zone and I.Z.: Internal Zone.

E–W. More to the south, over the Betics, the dimensionality is more complex with 3-D/2-D1-D, 2-D, 3-D/2-D and 3-D cases. The bidimensional structures (affected or not by galvanic distortion) can be classified in two groups with perpendicular strike directions, one oriented between E–W and WNW–ESE and the other with directions between N–S and NNE–SSW. Finally, the sites located over the Cenozoic basins (Guadix and Guadalquivir) are characterized by the presence of 1-D cases that are restricted to periods shorter than 0.1 s.

Between 1 and 10 s (band 4, Fig. 8d), the structure becomes more 3-D. The bidimensional cases are scarcer, less precise and located in the internal zone of the Betics (the southeastern part of the studied area) where they also show NNE–SSW and WNW–ESE strike directions.

These orthogonal bidimensional structures disappear for periods longer than 10 s at the same time that the dimensionality becomes essentially 3-D. Despite the predominance of this 3-D dimensionality, the presence for periods between 10 and 100 s (band 5, Fig. 8e) of relatively abundant bidimensional cases (affected by galvanic distortion) should be noted for the sites located over the Iberian Massif and external Betics. These cases show a NE–SW strike direction which is nearly parallel to that observed for shorter periods in the Iberian Massif.

For the longest periods, 100 s and greater (bands 6 and 7, Figs 8f and g), the dimensionality can only be determined at some sites located over the Betic Chain and is in general 3-D, with some 2-D cases at band 6 (Fig. 8f) with a high percentage of error.

6 DISCUSSION

Comparison between the observed geoelectric behaviour and the geological structure of the area denotes a good correlation at upper and middle crustal levels between the changes in the magnetotelluric dimensionality and the kind of deformation affecting the crust. The boundary between the autochthonous Iberian Massif and the allochthonous Betic Chain belongs to a thrust which dips towards the SSE beneath the internal zone and becomes nearly flat at a depth of about 5 km beneath the external zone (Banks & Warburton 1991). This autochthonous/allochthonous boundary coincides with the most significant change of the dimensionality signature recorded in the analysed data.

Thus, in the allochthonous zones, the dimensionality is highly variable with 2-D, 3-D/2-D, distorted 3-D and clearly 3-D structures and the strikes show two predominant directions: N–S to NNE–SSW and E–W to WNW–ESE. This signature could be related to the strong Alpine deformation present in this domain which, superimposed upon a previously Hercynian deformed basement in the internal zone, gave rise to the superimposition of folds and faults of different orientation (Azañón *et al.* 2002).

Beneath this domain, the upper crustal levels of the autochthonous zone are both 3-D and 2-D with a ENE-WSW strike. This simpler signature can be correlated with the Hercynian structure present in this sector of the Iberian Massif which is characterized by the presence of large E–W to ENE–WSW oriented structural domains (i.e. the Ossa-Morena zone) cut by large plutonic bodies with any preferred orientation.

A comparison between this domain and the allochthonous one indicates that the differences in the geoelectrical dimensionality between both domains are related not to the age of deformation but to the major tectonic complexity of the Betic Chain in relation of the Iberian Massif. Whereas the structure of the Iberian Massif is, on a large scale, mainly bidirectional, the structure of the Betic Chain is characterized by the development of faults and folds which often show changes in direction and are of minor scale.

For the longest periods ($>$100 s), in which the inductive length scale is of the same order as the length of the geological structures, the dimensionality is 3-D and it is not possible to distinguish the two domains. Lateral continuity of the conductive body beneath the internal zone in the previous NW–SE 2-D model (Pous *et al.* 1999) is not ensured because the dimensionality obtained is not 2-D on a large scale. A further 3-D interpretation should shed light on its extension and geodynamic significance.

7 CONCLUSIONS

A complete study of geoelectric dimensionality using real data and taking into account the errors is presented in this paper. Three different approaches, classical error propagation, random noise generation and resampling methods, provide similar estimations of the invariants and their errors. Random noise generation is more suitable for computing the errors of the parameters related to trigonometric functions (strike angles and distortion parameters). The threshold value used to distinguish between different kinds of dimensionality was tested for real data and we suggest a value between 0.1 and 0.15, for which the dimensionality is stable.

With regard to the dimensionality analysis using WAL invariants in the Betic Chain, we obtained information from 70 per cent of the data, which is sufficient to make a further 3-D interpretation.

The geoelectric structures are mainly 3-D. Some 1-D cases are located over the basins at short periods. Bidimensional structures with N–S to NNE–SSW and E–W to WNW–ESE orientations are found in the allochthonous zones, and with E–W to ENE–WSW in the autochthonous zones.

The complex dimensionality of the Betic Chain is related to the superimposition of processes that took part in its evolution, whereas the Iberian Massif, only affected by the Hercynian deformation, shows a simpler dimensionality.

ACKNOWLEDGMENTS

This work was supported by the Ministerio de Ciencia y Tecnología, Spain, projects REN 2002-4538-C02-01, RTE2001-1734-C03-03 and BTE2001-3650, and the Generalitat de Catalunya (GR 'Geodinàmica i Anàlisi de Conques' 2001SGR-00074). J. Ledo, A. Marcuello and J. T. Weaver provided helpful comments on this work.

REFERENCES

Azañón, J.M., Galindo-Zaldívar, J., García-Dueñas, V. & Jabaloy, A., 2002. Alpine tectonics II: Betic Cordillera and Balearic Islands, in *The Geology of Spain* eds Gibbons, W. & Moreno, T., pp. 401–416, Geological Society, London.

Bahr, K., 1988. Interpretation of the magnetotelluric impedance tensor: regional induction and local telluric distortion, *J. Geophys.,* **62,** 119–127.

Bahr, K., 1991. Geological noise in magnetotelluric data: a classification of distortion types, *Phys. Earth planet. Interior,* **66,** 24–38.

Banks, C.J. & Warburton, J., 1991. Mid crustal detachment in the Betic system of southeast Spain, *Tectonophysics.* **191,** 275–289.

Berdichevsky, M.N. & Dmitriev, V.I., 1976. Basic principles of interpretation of magnetotelluric curves, in *Geoelectric and Geothermal Studies*, KAPG Geophysical Monograph, pp. 165–221, ed. Á. Ádam, Akademiai Kaido, Budapest.

Carbonell, R., Sallarés, V., Pous, J., Dañobeitia, J.J., Queralt, P., Ledo, J.J. & García-Dueñas, V., 1998. A multidisciplinary study in the Betic Chain, *Tectonophysics,* **288,** 137–152.

Efron, B. & Tibshirani, R.J., 1998: An introduction to the bootstrap., *Monographs on Statistics and Applied Probability*, **57,** CRC, Boca Raton, FL.

Fischer, G. & Masero, W., 1994. Rotational properties of the magnetotelluric impedance tensor: the example of the Araguainha impact crater, Brazil, *Geophys. J. Int.,* **119,** 548–560.

Gamble, T.D., Goubau, W.M. & Clarke, J., 1979. Error analysis for remote reference magnetotellurics, *Geophysics,* **44,** 959–968.

Garcia-Dueñas, V., Balanyá, J.C. & Martínez-Martínez, J., 1992. Miocene extensional detachment in the outcropping basement of the Northern Alboran basin (Betics) and their tectonic implications, *Geo-Mar. Lett.,* **12,** 88–95.

García-Hernández, M., López-Garrido, A.C., Rivas, P., Sanz de Galdeano, C. & Vera, J., 1980. Mesozoic paleogeographic evolution in the External Zones of the Betic Cordillera (Spain), *Geol. Mijnbouw,* **59,** 155–168.

Groom, R.W. & Bailey, R.C., 1989. Decomposition of the magnetotelluric impedance tensor in the presence of local three-dimensional galvanic distortion, *J. geophys. Res.,* **94,** 1913–1925.

Groom, R.W. & Bailey, R.C., 1991. Analytic investigations of the effects of near-surface three dimensional galvanic scatterers on MT tensor decompositions, *Geophysics,* **56,** 496–518.

Jiracek, G., 1990. Near-surface and topographic distortions in electromagnetic induction, *Surv. Geophys.,* **11,** 163–203.

Johnson, C., Harbury, N. & Hurford, A.J., 1997. The role of extension in the Miocene denudation of the Nevado-Filabride Complex, Betic Cordillera (SE Spain), *Tectonics,* **16,** 189–204.

Jones, A.G., 1983. The problem of current channelling, a critical review. *Geophys. Surv.,* **6,** 79–122.

Jones, A.G. & Groom, R.W., 1993. Strike angle determination from the magnetotelluric impedance tensor in the presence of noise and local distortion: rotate at your peril! *Geophys.*, *J. Int.,* **113,** 524–534.

Ledo, J., 2004. 2-D versus 3-D magnetotelluric data interpretation, *Surveys in Geophys.,* in press.

Ledo, J., Queralt, P., Martí, A. & Jones, A.G., 2002. Two-dimensional interpretation of three-dimensional magnetotelluric data, an example of limitations and resolution, *Geophys. J. Int.,* **150,** 127–139.

Lezaeta, P., 2002. Confidence limit of the magnetotelluric phase sensitivity skew, *Earth planets Space,* **54,** 451–457.

Lilley, F.E.M., 1993. Magnetotelluric analysis using Mohr circles, *Geophysics,* **58,** 1498–1506.

Lilley, F.E.M., 1998a. Magnetotelluric tensor decomposition: 1. Theory for a basic procedure, *Geophysics,* **63,** 1884–1897.

Lilley, F.E.M., 1998b. Magnetotelluric tensor decomposition: 2. Examples of a basic procedure, *Geophysics,* **63,** 1898–1907.

Marquis, G., Jones, A.G. & Hyndman, R.D., 1995. Coincident conductive & reflective lower crust across a thermal boundary in southern British Columbia, Canada, *Geophys. J. Int.,* **120,** 111–131.

McNeice, G.W. & Jones, A.G., 2001. Multisite, multifrequency tensor decomposition of magnetotelluric data, *Geophysics,* **66,** 158–173.

Park, S.K. & Mackie, R.L., 2000. Resistive (dry?) lower crust in an active orogen, Nanga Parbat, northern Pakistan, *Tectonophysics,* **316,** 359–380.

Platt, J.P. & Vissers, R.L.M., 1989. Extensional collapse of thickened continental lithosphere: A working hypothesis for the Alboran Sea and the Gibraltar arc, *Geology,* **17,** 540–543.

Pous, J., P. Queralt, J.J. Ledo & Roca, E., 1999. A high electrical conductive zone at lower crustal depth beneath the Betic Chain (Spain), *Earth planet. Sci. Lett.,* **167,** 35–45.

Sanz de Galdeano, C. & Vera, J.A., 1992. Stratigraphic record and palaeogeographical context of the Neogene basins in the Betic Cordillera, Spain, *Basin Res.,* **4,** 21–36.

Smith, J.T., 1995. Understanding telluric distortion matrices, *Geophys. J. Int.,* **122,** 219–226.

Swift, C. M., 1967. Magnetotelluric investigation of an electrical conductivity anomaly in the southwestern United States, *PhD thesis*, Department of Geology and Geophysics, MIT, Cambridge, MA. (Reprinted in Vozoff, K. (ed.), 1988. *Magnetotelluric Methods*, Geophysics Reprint Series no 5, pp. 156–166, Society of Exploration Geophysicists, Tulsa, OK.)

Szarka, L., 1999. A correction to Bahr's 'phase deviation' method for tensor decomposition, *Earth planets Space,* **51,** 1019–1022.

Szarka, L. & Menvielle, M., 1997. Analysis of rotational invariants of the magnetotelluric impedance tensor, *Geophys. J. Int.,* **129,** 133–142.

Vozoff, K., 1972. The magnetotelluric method in the exploration of sedimentary basins, *Geophysics,* **19,** 281–289.

Vozoff, K. (ed.), 1986. *Magnetotelluric Methods*, Geophysics Reprint Series no 5, Society of Exploration Geophysicists, Tulsa, OK.

Vozoff, K., 1991. The magnetotelluric method, in *Electromagnetic Methods Applied in Geophysics*, Vol. 2, ed. Nabighian, M. N., pp. 641–711, Society of Exploration Geophysicists, Tulsa, OK.

Wannamaker, P.E., 1999. Affordable magnetotellurics: interpretations in natural environments, in *Three-Dimensional Electromagnetics,* eds Oristaglio, M. & Spies, B., pp. 349–374, Society of Exploration Geophysicists, Tulsa, OK.

Weaver, J.T., Agarwal, A.K. & Lilley, F.E.M., 2000. Characterisation of the magnetotelluric tensor in terms of its invariants, *Geophys. J. Int.,* **141,** 321–336.

APPENDIX

To obtain the analytical expression of the errors of each invariant, classical error propagation was applied to equations 4 to 8, regarding the errors of the tensor components M_{ij} as statistically independent. The expression are shown in terms of ξ_i and η_i and their errors:

$$\delta\xi_1 = \delta\xi_3 = \frac{1}{2}\sqrt{\delta\mathrm{Re}M_{xx}^2 + \delta\mathrm{Re}M_{yy}^2} \tag{A-1a}$$

$$\delta\xi_2 = \delta\xi_4 = \frac{1}{2}\sqrt{\delta\mathrm{Re}M_{xy}^2 + \delta\mathrm{Re}M_{yx}^2} \tag{A-1b}$$

$$\delta\eta_1 = \delta\eta_3 = \frac{1}{2}\sqrt{\delta\mathrm{Im}M_{xx}^2 + \delta\mathrm{Im}M_{yy}^2} \tag{A-1c}$$

$$\delta\eta_2 = \delta\eta_4 = \frac{1}{2}\sqrt{\delta\mathrm{Im}M_{xy}^2 + \delta\mathrm{Im}M_{yx}^2} \tag{A-1d}$$

$$\delta I_1 = \frac{1}{I_1}\sqrt{\xi_1^2\delta\xi_1^2 + \xi_4^2\delta\xi_4^2} \tag{A-2}$$

$$\delta I_2 = \frac{1}{I_2}\sqrt{\eta_1^2\delta\eta_1^2 + \eta_4^2\delta\eta_4^2} \tag{A-3}$$

$$\delta I_3 = \frac{1}{I_1^2 I_3}\sqrt{\xi_2^2\delta\xi_2^2 + \xi_3^2\delta\xi_3^2} + \frac{I_3}{I_1^2}\sqrt{\xi_1^2\delta\xi_1^2 + \xi_4^2\delta\xi_4^2} \tag{A-4}$$

$$\delta I_4 = \frac{1}{I_2^2 I_4}\sqrt{\eta_2^2\delta\eta_2^2 + \eta_3^2\delta\eta_3^2} + \frac{I_4}{I_2^2}\sqrt{\eta_1^2\delta\eta_1^2 + \eta_4^2\delta\eta_4^2} \tag{A-5}$$

$$\delta I_5 = \delta s_{41} = \frac{1}{I_1 I_2}\sqrt{\left(\eta_4 - I_5\xi_1\frac{I_2}{I_1}\right)^2\delta\xi_1^2 + \left(\eta_1 - I_5\xi_4\frac{I_2}{I_1}\right)^2\delta\xi_4^2 + \left(\xi_4 - I_5\eta_1\frac{I_1}{I_2}\right)^2\delta\eta_1^2 + \left(\xi_1 - I_5\eta_4\frac{I_1}{I_2}\right)^2\delta\eta_4^2} \tag{A-6}$$

$$\delta d_{ij} = \frac{1}{I_1 I_2}\sqrt{\left(\eta_j - d_{ij}\xi_i\frac{I_2}{I_1}\right)^2\delta\xi_i^2 + \left(-\eta_i - d_{ij}\xi_j\frac{I_2}{I_1}\right)^2\delta\xi_j^2 + \left(-\xi_j - d_{ij}\eta_i\frac{I_1}{I_2}\right)^2\delta\eta_i^2 + \left(\xi_i - d_{ij}\eta_j\frac{I_1}{I_2}\right)^2\delta\eta_j^2} \tag{A-7}$$

$$\delta I_6 = \delta d_{41} = \frac{1}{I_1 I_2}\sqrt{\left(\eta_1 - I_6\xi_4\frac{I_2}{I_1}\right)^2\delta\xi_4^2 + \left(-\eta_4 - I_6\xi_1\frac{I_2}{I_1}\right)^2\delta\xi_1^2 + \left(-\xi_1 - I_6\eta_4\frac{I_1}{I_2}\right)^2\delta\eta_4^2 + \left(\xi_4 - I_{41}\eta_1\frac{I_1}{I_2}\right)^2\delta\eta_1^2} \tag{A-8}$$

$$\delta Q = \sqrt{\sum_{k=1}^{4}\left[\left(\sum_{\substack{ij=12,\\13,24,34}}\frac{\partial Q}{\partial d_{ij}}\frac{\partial d_{ij}}{\partial\xi_k}\right)^2\delta\xi_k^2 + \left(\sum_{\substack{ij=12,\\13,24,34}}\frac{\partial Q}{\partial d_{ij}}\frac{\partial d_{ij}}{\partial\eta_k}\right)^2\delta\eta_k^2\right]} \tag{A-9}$$

$$\delta I_7 = \sqrt{\sum_{k=1}^{4}\left[\left(\frac{\partial I_7}{\partial Q}\sum_{\substack{ij=12,\\13,24,34}}\frac{\partial Q}{\partial d_{ij}}\frac{\partial d_{ij}}{\partial\xi_k} + \frac{\partial I_7}{\partial d_{41}}\frac{\partial d_{41}}{\partial\xi_k} + \frac{\partial I_7}{\partial d_{23}}\frac{\partial d_{23}}{\partial\xi_k}\right)^2\delta\xi_k^2 + \left(\frac{\partial I_7}{\partial Q}\sum_{\substack{ij=12,\\13,24,34}}\frac{\partial Q}{\partial d_{ij}}\frac{\partial d_{ij}}{\partial\eta_k} + \frac{\partial I_7}{\partial d_{41}}\frac{\partial d_{41}}{\partial\eta_k} + \frac{\partial I_7}{\partial d_{23}}\frac{\partial d_{23}}{\partial\eta_k}\right)^2\delta\eta_k^2\right]} \tag{A-10}$$

with:

$$\frac{\partial Q}{\partial d_{12}} = \frac{1}{Q}(d_{12} - d_{34}) \quad \text{and} \quad \frac{\partial Q}{\partial d_{34}} = -\frac{1}{Q}(d_{12} - d_{34}) \tag{A-11}$$

$$\frac{\partial Q}{\partial d_{13}} = \frac{\partial Q}{\partial d_{24}} = \frac{1}{Q}(d_{13} + d_{24}) \tag{A-12}$$

$$\frac{\partial d_{ij}}{\partial\xi_k} = \frac{1}{I_1 I_2}\left\{\begin{array}{lll} \eta_j, & k = i & \\ -\eta_i, & k = j & \\ 0, & & k \neq i \neq j \end{array}\right\} - d_{ij}\frac{1}{I_1}\left\{\begin{array}{ll} \xi_k/I_1, & k = 1,4 \\ 0, & k = 2,3 \end{array}\right\} \tag{A-13}$$

$$\frac{\partial d_{ij}}{\partial\eta_k} = \frac{1}{I_1 I_2}\left\{\begin{array}{lll} -\xi_j, & k = i & \\ \xi_i, & k = j & \\ 0, & & k \neq i \neq j \end{array}\right\} - d_{ij}\frac{1}{I_2}\left\{\begin{array}{ll} \eta_k/I_2, & k = 1,4 \\ 0, & k = 2,3 \end{array}\right\} \tag{A-14}$$

$$\frac{\partial I_7}{\partial Q} = -\frac{1}{Q^2}(d_{41} - d_{23}) \tag{A-15}$$

$$\frac{\partial I_7}{\partial d_{41}} = \frac{1}{Q} \quad \text{and} \quad \frac{\partial I_7}{\partial d_{23}} = \frac{-1}{Q} \tag{A-16}$$